Christopher Beaudoin et al.: Post-correlation Processing for the VLBI2010 Proof-of-concept System, IVS 2010 General Meeting Proceedings, p.35–39
http://ivscc.gsfc.nasa.gov/publications/gm2010/beaudoin2.pdf

Post-correlation Processing for the VLBI2010 Proof-of-concept System

Christopher Beaudoin, Arthur Niell

MIT Haystack Observatory

Contact author: Christopher Beaudoin, e-mail: cbeaudoin@haystack.mit.edu

Abstract

For the past three years, the MIT Haystack Observatory and the broadband team have been developing a proof-of-concept broadband geodetic VLBI microwave (2-12 GHz) receiver. Also on-going at Haystack is the development of post-correlation processing needed to extract the geodetic observables. Using this processing, the first fully-phase-calibrated geodetic fringes have been produced from observations conducted with the proof-of-concept system. The results we present show that the phase-calibrated phase residuals from four 512 MHz bands spanning 2 GHz have an RMS phase variation of 8^o which corresponds to a delay uncertainty of 12 ps.

1. Raw Fringe Phasor Model

This development begins by assuming that one has at their disposal the normalized correlation coefficients for each frequency channel (whether represented in the cross-power frequency or lag domain) for each single correlator accumulation period (AP). The raw fringe phasor $\Phi_r(f)$ is then defined as the phase of the cross-power spectrum produced from the correlator output data and is assumed to be the product of the fringe phasor $\Phi_g(f)$ due to the residual geodetic delay and the hardware (phase cal) phasor $\Phi_{pc}(f)$, where f is the sky frequency. Furthermore, since amplitudes are currently not incorporated in the phase cal processing, the magnitude of all phasors considered in this note are arbitrarily set to unity.

The hardware-related phase is given by the phase calibration phasor $\Phi_{pc}(f)$ which represents the arithmetic difference between the phase cal phases obtained at each station. $\Phi_{pc}(f)$ is also sampled every $f = 5n$ MHz, where n is the rail harmonic number. In the context of this note, $\Phi_{pc}(f)$ will be modeled as a piecewise-linear phasor function composed of as many pieces as there are frequency channels as indicated in Figure 1. It is important to note that $\Phi_{pc}(f)$ is not simply the difference of the phase cal phases obtained directly from the correlator, since the pcal phases are sampled every 5 MHz and the fringe phases in each frequency channel, generally, are sampled at a different rate. Additional processing (interpolation) is needed to obtain $\Phi_{pc}(f)$ from the correlator pcal phases. This is discussed in the section on phase calibration fitting.

In regards to the phase due to the residual geodetic delay, systematic errors such as those introduced by clock drift and ionosphere delay are neglected here to place emphasis on the phase calibration processing needed to connect the raw fringe phases across several receiver bands. The residual geodetic fringe phasor (i.e., the error-free fringe phase), represented by the function $\Phi_g(f)$, is assumed to be linear in frequency since the aforementioned errors are ignored; estimation of $\Phi_g(f)$ from knowledge of $\Phi_r(f)$ and $\Phi_{pc}(f)$ is the goal of the correlator post-processing described in this paper. $\Phi_g(f)$ can be formally written as:

$$\Phi_g(f) = e^{2\pi f \tau_g} \tag{1}$$

where τ_g is the residual time delay (between the two stations) to the geodetic model. Under this development the raw fringe phase is assumed to be the product of the geodetic and phase cal phasors:

$$\Phi_r(f) = \Phi_g(f)\Phi_{pc}(f) \tag{2}$$

Figure 1 displays a graphical example of the phases $\Phi_r(f)$, $\Phi_{pc}(f)$, and $\Phi_g(f)$ for the current receiver architecture (eight 32 MHz channels per band and four 512 MHz bands) and band-to-band spacings Δf_1 through Δf_3.

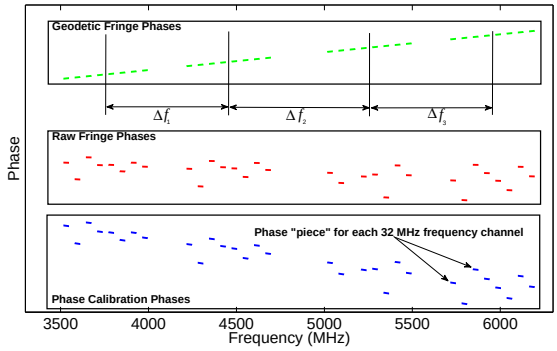

Figure 1. Graphical representation of geodetic fringe, raw fringe, and phase calibration phases.

2. Phase Calibration Phase Fitting - Derivation of $\Phi_{pc}(F)$

As mentioned previously, the phase cal tones are injected in the front-end of the receiver at frequencies which are multiples of 5 MHz whereas the frequencies at which the raw fringe phases are sampled, in general, are different. As a result, the phase cal data provided by the correlator must be fit to a model (linear in this case) in order that the phase calibration phases can be evaluated at the same sky frequencies as the raw fringe phases. The following model is used to describe the phase cal phasor provided by the correlator:

$$\Phi^m_{pc}(f)\Big|_{f=nf_r} = e^{2\pi n f_r \tau^m_{pc} + \phi^m_{pc}} \tag{3}$$

$\Phi^m_{pc}(f)$ describes the phase cal model for the mth frequency channel as a function of tone index n; in this model $\Phi^m_{pc}(f)$ represents the arithmetic difference of the phase cal phases (as provided by the correlator) between the two stations for the given channel. In equation (3), f_r is the rail frequency spacing (5 MHz) and τ^m_{pc} and ϕ^m_{pc} are the phase cal delay and phase, respectively, for the mth channel; f and therefore n are bounded by the frequencies of the channel from which the phase calibration tones were extracted. Given the samples of $\Phi^m_{pc}(f)$, the task is to estimate τ^m_{pc} and ϕ^m_{pc} which, by inspection of equation (3), can be accomplished by applying a discrete Fourier transform (DFT) to $\Phi^m_{pc}(f)$. The DFT makes no assumptions about the frequency locations of the tones in any given channel, so there is no restriction on the tone selection. After τ^m_{pc} and ϕ^m_{pc} have been estimated, the interpolated pcal phasor $\Phi^{mi}_{pc}(f)$ can be expressed using the same linear model in equation (3) by simply substituting for the tone frequency nf_r the sky frequency

f corresponding to that at which the raw fringe phasor is evaluated:

$$\Phi_{pc}^{mi}(f) = e^{2\pi f \tau_{pc}^{m} + \phi_{pc}^{m}} \tag{4}$$

The complete phase calibration phasor (assuming there is no overlap of the frequency channels) is just the sum of the interpolated pcal phasors for each frequency channel:

$$\Phi_{pc}(f) = \sum_{m} \Phi_{pc}^{mi}(f) \tag{5}$$

3. Phase Calibration Correction of Raw Fringe Phases

The raw fringe phasor $\Phi_r(f)$ and phase calibration phasor $\Phi_{pc}(f)$ are produced by the correlator after each accumulation period (AP); therefore, $\Phi_r^m(f)$ can be corrected for each AP independently (this is the so-called AP-by-AP pcal mode). The benefit of the AP-by-AP mode is that hardware drift over extended scan periods is removed. Equation (2) indicates that the residual geodetic phasor can be obtained by simply multiplying the raw fringe phasor by the complex conjugate of the phase calibration phasor:

$$\Phi_g(f) = \Phi_r(f)\Phi_{pc}^{*}(f) \tag{6}$$

For the polyphase filter implementation of the frequency channelization currently implemented in the digital backend, the sky frequency f can be decomposed into a summation of the LO frequencies of the channels and the cross-power frequency relative to the channel LO frequency. Formally put:

$$f \equiv f_{LO}^{m} - k\Delta f_{cpf} \tag{7}$$

where f_{LO}^{m} is the LO frequency of channel m, f_{cpf} is the cross-power frequency sample interval, k is the cross-power frequency index (i.e., 0,1,2,...N_{sc}-1), and N_{sc} is the number of cross-power spectral samples in a single 32 MHz frequency channel. Equation (6) can now be rewritten using equations (4-5,7) to provide a more detailed formulation of the method used to correct the raw fringe phases and obtain the residual geodetic phases:

$$\Phi_g(f) = \Phi_r(f) \sum_{m} e^{-j2\pi f_{LO}^{m} \tau_{pc}^{m}} \; e^{j2\pi k \Delta f_{cpf} \tau_{pc}^{m}} \; e^{-j\phi_{pc}^{m}} \tag{8}$$

4. Broadband Phase Calibration Processing of Experiment 3296

Since the goal of the broadband phase calibration processing is to remove the hardware-related delay and phase from the raw fringe phasor, broadband fringe tests have been conducted on the Westford-GGAO baseline to demonstrate the performance of this processing. The broadband system possesses the flexibility to change the inter-band spacings Δ_{f1} through Δ_{f3} (depicted in Figure 1) with 400 kHz precision. In fact, the inter-band spacings can be set identically to zero which provides a quite useful diagnostic for validating the broadband phase calibration processing as outlined in this note. In this so-called "overlapping bands" configuration, all four bands observe an identical set of frequency channels, and the residual geodetic fringe phasors for each band (fringe fit independently) are expected to be identical if the receiver is truly front-end noise limited. In practice, the residual geodetic fringe phasors must be coherently averaged over all APs in the integration period in order to detect the interference fringes. Table 1 displays the raw

Table 1. Raw singleband/multiband delays, fringe rate, and phase results from fringe fitting.

	A	**B**	**C**	**D**
Singleband Delay (ns)	-2.334	1.374	-10.086	-4.063
Multiband Delay (ns)	-1.970	1.768	6.011	-3.635
Fringe Rate (mHz)	1.522	2.216	2.016	2.043
Fringe Phase (^{o})	-157.7	-91.5	55.6	-72.2

Table 2. Phase-calibrated singleband/multiband delays, fringe rate, and phase results from fringe fitting.

	A	**B**	**C**	**D**
Singleband Delay (ns)	-0.503	0.180	-0.223	-0.241
Multiband Delay (ns)	0.076	0.069	0.083	0.092
Fringe Rate (mHz)	1.578	1.576	1.586	1.588
Fringe Phase (^{o})	-144.5	-142.5	-144.6	-143.6

singleband/multiband delays, fringe rate, and phase for HH polarization obtained from an observation conducted on Day258 at 1403UT year 2009 (Haystack Exp: 3296) coherently averaged over the entire 10 minute scan. In this experiment, all four bands observed 6408.4-6888.4 MHz. The raw fringe phasors processed without the broadband phase calibration method are given in Table 1 and the calibrated counterparts of those parameters are given in Table 2. The uncertainties associated with the singleband/multiband delay, fringe rate, and phase are 0.2 ns, 0.013 ns, 0.011 mHz, and 1.4^o, respectively. Comparison of Tables 1 and 2 demonstrates that the phase calibration processing is performing nearly as expected since the calibrated results for all four bands are in such good agreement; the minor discrepancies are under investigation.

During this same experiment, data were also collected such that the four bands spanned a total contiguous bandwidth of 2 GHz (6.4—8.4 GHz). Differences in cable lengths and local oscillator phases in the hardware comprising each frequency band introduce a hardware-related component to the raw residual fringe phase shown in Figure 2a. The discontinuities in Figure 2a appear at the spectral boundaries of adjacent frequency bands as a result of these hardware-related components. The raw data were phase calibrated using the technique described above, and the resultant calibrated fringe phases are shown in Figure 2b. As is obvious in comparing Figure 2a to 2b, the discontinuities are suppressed in the calibrated geodetic fringe phases. The resultant rms phase noise is 8.5^o, which translates to a delay uncertainty of 12 ps across the 2 GHz of contiguous bandwidth. This delay uncertainty will be reduced by observing larger spanned bandwidths and this is one of the explicit goals of VLBI2010.

5. Conclusions and Future Plans

In order to remove the hardware-related phase and delay components from the raw fringe phasors, a new phase calibration correction algorithm has been developed. This processing was shown to reconcile the band-to-band delay and fringe rate differences when all four bands observed the identical set of sky frequencies, thus demonstrating the algorithm's ability to remove the

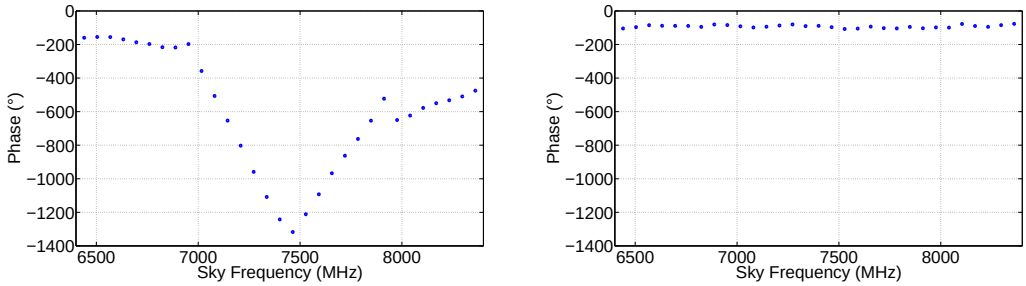

(a) Raw Fringe Phase (b) Calibrated Fringe Phase

Figure 2. Raw and Calibrated Residual Fringe Phase vs. Sky Frequency

hardware-related components of the aformentioned delay/rate parameters. Though the observable parameters are fairly consistent, Table 2 demonstrates that there are post-correction differences between the bands. Observation of such discrepancies suggests that additional independent noise is added to the signal recorded in each frequency band after the 2-12 GHz microwave signal received by the front-end is equally split into each of the four frequency bands (signal chain [1] pp. 35). A signal chain cascade analysis indicates that the noise contributed by the analog components in each frequency band is negligible. The noise contributed by the digital backend (DBE) (i.e., ADC, fixed point math quantization errors), however, is not currently a quantity that can be measured directly. As such, there may be significant noise contribution by the DBE of which we are unaware. This situation will be rectified with the introduction of the next-generation DBE, at which point a full signal chain (analog/digital) noise budget can be developed to assess the expected uncertainties in the band-to-band post-correction residuals.

The phase calibration correction algorithm was also shown to align the raw fringe phases across a total bandwidth of 2 GHz, which resulted in a delay uncertainty of 12 ps. In order to reduce the delay precision of the geodetic observables, future observations will be conducted which span bandwidths greater than 2 GHz. In observing these wider bandwidths the ionosphere is expected to introduce a dispersive (non-linear) behavior in the fringe phase function (e.g., Figure 2b) which will require modification of the fringe fitting routine from a linear model to one that is dispersive. Finally, the results reported in this paper were for the linear HH polarization only. Developments of the fringe fitting algorithm will also need to incorporate all four polarization components (HH, HV, VH, and VV) into the geodetic fringe fitting process in order to further enhance the SNR and realize the goals of VLBI2010 [1].

6. Acknowledgements

This development of the processing algorithm described in this work is the result of many discussions with Brian Corey and Bill Petrachenko. Many thanks to them for their contributions.

References

[1] B. Petrachenko, et. al., “Design Aspects of the VLBI2010 System,” International VLBI Service for Geodesy and Astrometry Annual Report 2008, NASA/TP-2009-214183, pp.13-66, July 2009